Journal of Power Sources 202 (2012) 276–283

Contents lists available at SciVerse ScienceDirect

Journal of Power Sources

journal homepage: www.elsevier.com/locate/jpowsour

Self-assembly of Co—Sb-nanocrystal/graphene hybrid nanostructure with improved Li-storage properties via a facile in situ solvothermal route

Yunxiao Zheng, Jian Xie*, Shuangyu Liu, Wentao Song, Gaoshao Cao, Tiejun Zhu, Xinbing Zhao

Department of Materials Science and Engineering, Zhejiang University, Hangzhou 310027, China

ARTICLE INFO

Article history:
Received 21 September 2011
Received in revised form 3 November 2011
Accepted 15 November 2011
Available online 9 December 2011

Keywords:
Graphene
Antimonides
Nanocomposite
Li-storage properties
In situ route

ABSTRACT

In this work, a Co—Sb-nanocrystal/graphene hybrid nanostructure has been synthesized by a facile one-pot in situ solvothermal route. X-ray diffraction and X-ray photoelectron spectroscopy analyses show that the formation of Co—Sb alloy (CoSb or $CoSb_2$) and the reduction of graphite oxide occur simultaneously during the one-pot solvothermal process. Scanning electron microscopy and transmission electron microscopy observations indicate that quasi-spheric CoSb (or $CoSb_2$) nanoparticles with a size of 10–30 nm are uniformly anchored on graphene, forming a unique layered structure. The presence of graphene prevents the nanoparticles from aggregating. The attached alloy nanoparticles also hinder the restacking of the graphene sheets. The electrochemical measurements have shown that Co—Sb-nanocrystal/graphene nanocomposites exhibit improved electrochemical Li-storage properties compared with bare Co—Sb alloy, due to the combined buffering, confining and conducting effects of the in situ introduced graphene.

1. Introduction

Graphene, a flat monolayer of sp^2-bonded two-dimensional (2D) carbon atoms, has received a great attention since first discovered by Novoselov et al. [1–3]. Due to its unique 2D single-layer nanostructure, graphene exhibits intriguing physicochemical properties such as high electronic conductivity (16,000 S m^{-1}) [4], high specific surface area (theoretical value of 2630 m^2 g^{-1}) [5] and high mechanical strength (~1100 GPa) [6]. These advantages make graphene a promising 2D support or building block for novel functional nanocomposites with potential applications in catalysis [7–9], biosensor [7,10], fuel cell [11–13], supercapacitor [14,15], and conductive polymer [16].

Currently, graphene has also been considered as an ideal matrix to support electrode materials for Li-ion batteries. Compared with conventional carbon anodes, Sn or Si-based anodes can yield a much higher capacity. However, these materials show a rapid capacity fade caused by the large volume changes during the Li-alloying/de-alloying processes. Recent researches on metals [17–20], oxides [21–26] and alloys [27,28] have shown that the electrochemical performance of these materials can be remarkably enhanced by loading them onto graphene. The flexible graphene acts not only as a buffer to accommodate the volume changes upon Li-alloying/de-alloying but also as a separator to refrain the aggregation of the nanoparticles during cycling. In addition, graphene exhibits a high electronic conductivity [4] and can yield a high Li-storage capacity [29].

Another merit of graphene is that its precursor, graphite oxide, is soluble in water or some polar solvents [30–32] and can be reduced by a solvothermal route [33–36]. In other words, graphite oxide is solution processable, which is compatible with the synthetic route for some nanosized Sb-based alloys [37–40]. Therefore, an in situ solution route can be used to synthesize a hybrid nanostructure constructed by graphene nanosheets and alloy nanoparticles. Herein, we report the preparation of Co—Sb-nanocrystals/graphene hybrid by a facile one-pot in situ solvothermal route. The microstructure, formation mechanism and electrochemical Li-storage properties of the nanocomposites will be investigated.

2. Experimental

2.1. Preparation of CoSb–graphene and $CoSb_2$–graphene nanocomposites

Graphite oxide (GO), prepared by a modified Hummer's method [41], was dissolved in 60 mL of ethylene glycol (EG) with sonication for 3 h to form a homogeneous dispersion. Then, 2 mmol of $CoCl_2 \cdot 6H_2O$ and 2 mmol of $SbCl_3$ (4 mmol for $CoSb_2$) were added to the above dispersion with sonication for another 0.5 h. The GO/Co + Sb (or Co + 2Sb) weight ratio is 1:5. A sufficient amount of $NaBH_4$ was then added slowly to the above mixed solution. The

* Corresponding author. Tel.: +86 571 87952181; fax: +86 571 87951451.
E-mail address: xiejian1977@zju.edu.cn (J. Xie).

0378-7753/$ – see front matter © 2011 Elsevier B.V. All rights reserved.
doi:10.1016/j.jpowsour.2011.11.049

mixture was transferred to a Teflon-lined stainless steel autoclave and heated in an electric oven at 220 °C for 24 h (230 °C, 48 h for $CoSb_2$). The resulting products were separated by centrifugation, washed with deionized water and dried at 30 °C under vacuum overnight. The obtained products are named CoSb/G and $CoSb_2$/G, where G represents graphene. For comparison, bare CoSb and bare $CoSb_2$ were also prepared using the same route without the addition of GO. A similar solvothermal route was also used to synthesize bare graphene.

2.2. Physicochemical characterization

The crystalline phases of the solvothermal products were characterized by X-ray diffraction (XRD) on a Rigaku D/Max-2550pc powder diffractometer equipped with Cu Kα radiation (λ = 0.1541 nm). X-ray photoelectron spectra (XPS) were recorded on a KRATOS AXIS ULTRA-DLD spectrometer with a monochromatic Al Kα radiation (*hv* = 1486.6 eV). The morphologies of the products were observed by field-emission scanning electron microscopy (FE-SEM) on a FEI-sirion microscope, transmission electron microscopy (TEM) and high-resolution TEM (HRTEM) on a JEM 2100F microscope.

2.3. Electrochemical measurements

The electrochemical properties of the products were evaluated by galvanostatic cycling using CR2025-type coin cells. The active material (CoSb/G, CoSb/G2, CoSb, $CoSb_2$/G or $CoSb_2$), acetylene black, polyvinylidene fluoride (PVDF) (75:15:10 in weight) were homogeneously mixed in N-methyl pyrrolidone (NMP) with magnetic stirring to form a slurry. The slurry was then pasted onto Ni foam to make the working electrodes. After drying at 100 °C under vacuum for 8 h, the working electrodes were assembled into half cells in an Ar-filled glove box using metallic Li foil as the counter electrode and Celgard 2300 microporous film as the separator. The electrolyte was 1 M $LiPF_6$ in ethylene carbonate (EC)/dimethyl carbonate (DMC) (1:1 in volume). The cells were charged and discharged on a LHS-B-5V5mA8D battery cycler (Wuhan, China) between 0.05 and 1.5 V (vs. Li/Li^+) at various current densities. Cyclic voltammetry (CV) measurements were performed on an Arbin BT2000 system over a voltage range 0.05–2.0 V (vs. Li/Li^+) at various scan rates. Electrochemical impedance spectroscopy (EIS) measurements were conducted on a CHI660C electrochemistry workstation. The impedance plots were collected by applying an AC signal of 5 mV amplitude over the frequency range from 10^{-2} to 10^5 Hz at de-lithiation state. All of the electrochemical measurements were performed at 25 °C.

3. Results and discussion

The formation mechanism of CoSb/G and $CoSb_2$/G hybrid nanostructures is schematically illustrated in Fig. 1. The formation process is as follows: first, the graphite oxide is sufficiently exfoliated into graphene oxide in EG by sonication; second, the Co^{2+} and Sb^{3+} are uniformly dispersed on the negatively charged graphene oxide [31] by electrostatic attraction; third, the graphene oxide is reduced to graphene, and the metal ions (Co^{2+} and Sb^{3+}) are reduced to metals (Co and Sb) by $NaBH_4$ followed by the formation of CoSb or $CoSb_2$; finally, graphene sheets loaded with CoSb (or $CoSb_2$) nanoparticles are self-assembled into layered CoSb–graphene (or $CoSb_2$–graphene) hybrid nanostructure by confining CoSb (or $CoSb_2$) nanoparticles in between the graphene sheets due to the hydrophobic nature of graphene. The firmly attached nanoparticles, on the other hand, can act as spacers to prevent the graphene sheets from restacking.

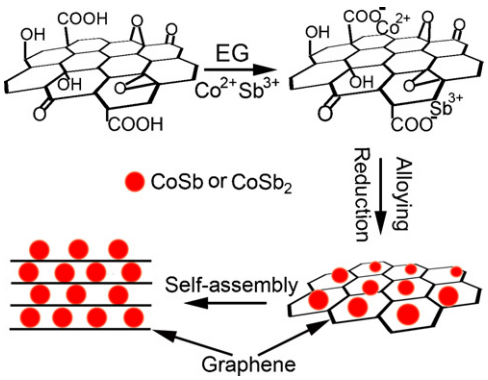

Fig. 1. Schematic illustration of the formation mechanism of CoSb/G and $CoSb_2$/G.

Fig. 2a shows the XRD patterns of CoSb/G and bare CoSb. All the diffraction peaks can be indexed to hexagonal CoSb phase (space group $P6_3/mmc$, JCPDS No. 33-0097) for both CoSb/G and bare CoSb. The diffraction peaks related to graphene is undetectable, indicating that the restacking of the graphene sheets after reduction is refrained by uniformly loading CoSb nanoparticles in between the graphene sheets, in agreement with the formation mechanism of CoSb/G discussed above. Fig. 2b shows the SEM image of a CoSb/G flake. Through the transparent graphene, it is clear that nanosized CoSb particles are homogeneously confined in between the graphene sheets. A layered structure with alternating CoSb-nanoparticles and graphene-nanosheets is evident from the broken cross section of the flake (denoted by the arrows), agreeing with the proposed formation mechanism in Fig. 1.

TEM image in Fig. 2c indicates that the CoSb nanoparticles with a size of 20–40 nm are uniformly anchored on graphene. The graphene is rather thin evidenced by the transparent nature and the surface wrinkles. Fig. 2d demonstrates the lattice-resolved HRTEM image of an individual CoSb particle anchored on graphene. The fringe spacing is measured to be 0.28 nm, corresponding to the inter-planar spacing of (1 0 1) plane of CoSb. The fringes with a spacing of 0.38 nm correspond to the (0 0 2) plane of graphene.

Fig. 3a shows the XRD patterns of $CoSb_2$/G and bare $CoSb_2$ prepared at 230 °C for 48 h in EG. The dominant diffraction peaks can be indexed to monoclinic $CoSb_2$ phase (space group $P2_1/c$, JCPDS No. 29-0126) for both the products. For $CoSb_2$/G, minor diffraction CoSb peaks are also observed. For bare $CoSb_2$, Sb is also observed besides CoSb. It seems that the addition of graphene facilitates the formation of $CoSb_2$. The absence of the graphene peaks also indicates that the graphene sheets are completely exfoliated by the attached $CoSb_2$ particles to form a $CoSb_2$/G layered structure. The formation of the layered structure is confirmed by the SEM observation as seen in Fig. 3b. TEM image (Fig. 3c) shows that the $CoSb_2$ nanocrystals with a size of around 20 nm are uniformly loaded on the transparent graphene. The HRTEM image in Fig. 3d verifies the good crystallization of $CoSb_2$ even though synthesized at a low temperature.

XPS measurements were performed to check whether graphite oxide has been reduced to graphene during the solvothermal process. Fig. 4 gives the C1s XPS of graphite oxide, CoSb/G and $CoSb_2$/G. The XPS can be fitted into four peaks, corresponding to carbon atoms in four functional groups: sp^2 carbon (C—C, 284.8 eV), carbon in C—O group (epoxide or hydroxyl, 286.3 eV), carbonyl carbon (C=O, 287.6 eV) and carboxylate carbon (O—C=O, 289.0 eV) [42,43]. Note that the peak intensity of carbons in C—O, C=O and O—C=O groups exhibits a significant decrease in CoSb/G or $CoSb_2$/G compared with that in graphite oxide, indicative of a considerable reduction of graphite oxide into graphene during the solvothermal reaction. It should be stressed that the solvothermal products

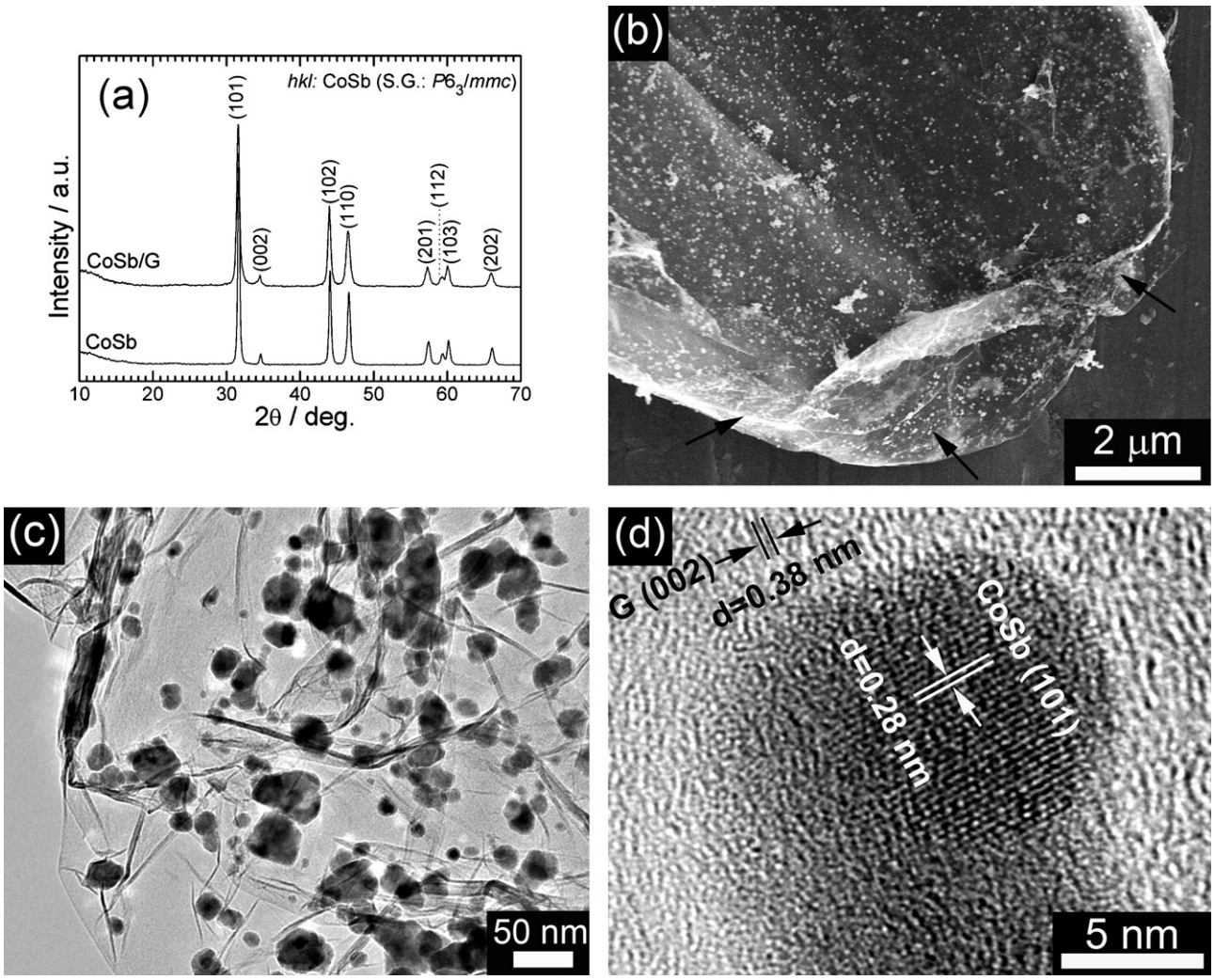

Fig. 2. (a) XRD patterns of CoSb/G and bare CoSb, (b) SEM, (c) TEM and (d) HRTEM images of CoSb/G.

still contain residual epoxide and/or hydroxyl groups, in consistency with the theoretical calculation that these groups are difficult to remove when located at the edges of the graphite oxide [44]. Similar phenomenon was also observed in graphene prepared also using $NaBH_4$ as the reductant [45]. From the XRD, SEM, TEM, and XPS analyses, it can be concluded that CoSb/G and $CoSb_2$/G hybrid nanostructures have formed by this facile one-pot in situ solvothermal route.

The morphologies of graphene, bare CoSb and bare $CoSb_2$ are also observed to understand their interaction mechanism during the formation of the layered CoSb/G and $CoSb_2$/G. We found that hydrophobic graphene sheets show a strong tendency to restack without the attachment of CoSb or $CoSb_2$ nanoparticles. On the other hand, both CoSb and $CoSb_2$ nanoparticles tend to aggregate without the confinement of graphene. These observations further confirm the formation mechanism of the hybrid nanostructure shown in Fig. 1.

Fig. 5a presents the charge–discharge curves of CoSb and CoSb/G for the first three cycles at 40 mA g^{-1}. The first charge (Li-extraction) and discharge (Li-absorption) of bare CoSb are 490 and 643 mAh g^{-1}. Compared with bare CoSb, CoSb/G yields a lower first charge capacity of 444 mAh g^{-1} and a higher first discharge capacity of 694 mAh g^{-1}. This is due to the fact that graphene itself gives a low first charge capacity and a high first discharge capacity as shown in Fig. 5d. Fig. 5b shows the CV plots of bare CoSb and CoSb/G for the first three scans at 0.1 mV s^{-1}. The oxidation and reduction peaks, which located at around 1.2 and 0.6 V, respectively, correspond to the charge and discharge plateaus in Fig. 5a. It is apparent that CoSb/G exhibits a better electrochemical reversibility than bare CoSb evidenced from its almost overlapped charge–discharge curves or CV plots after the first cycle. Note that during the first discharge process, CoSb/G shows a higher potential plateau than bare CoSb, due possibly to the interaction between CoSb nanoparticles and graphene.

Fig. 5c compares the cycling stability between bare CoSb and CoSb/G. For comparison, the cycling performance of another CoSb–graphene sample (CoSb/G2), prepared using the precursors with a high GO/Co + Sb weight ratio (3:10), is also given. As seen in the figure, CoSb/G shows an improved cycling stability than bare CoSb especially in the initial 30 cycles. The improvement in cycling stability can be attributed to the introduction of graphene that acts both as a buffer to accommodate the volume changes upon Li-absorption/extraction into/from CoSb and as a separator to prevent the CoSb nanoparticles from aggregating. The long-term cycling stability of CoSb/G, however, is not satisfactory yet, probably because of the intrinsic large volumes of CoSb and/or the gradually weakened buffering/separating ability of graphene. Note that CoSb/G2 demonstrates an obviously better cycling stability than CoSb/G, implying that graphene indeed plays a crucial role in enhancing the cycling stability of CoSb alloy. It is worth noting that the increase in current density only exerts a slight influence on the cycling stability for CoSb/G2, while for bare CoSb and CoSb/G,

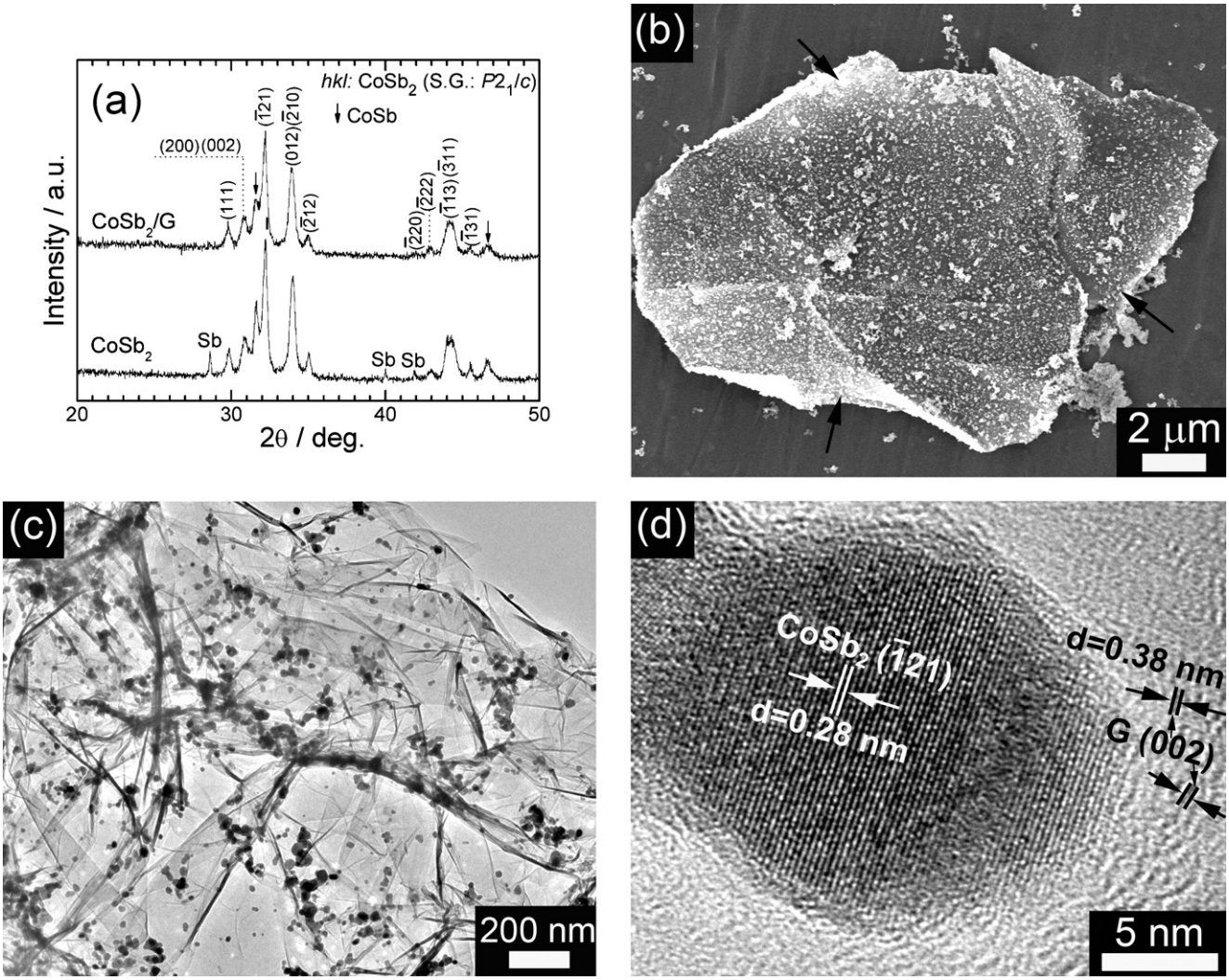

Fig. 3. (a) XRD patterns of $CoSb_2$/G and bare $CoSb_2$, (b) SEM, (c) TEM and (d) HRTEM images of $CoSb_2$/G.

increasing the current density leads to the degraded cycling stability significantly.

Fig. 6a displays the charge–discharge curves of $CoSb_2$ and $CoSb_2$/G for the first three cycles. Similar to CoSb/G, $CoSb_2$/G also gives a lower first charge capacity (558 mAh g^{-1}) and a higher first discharge capacity (849 mAh g^{-1}) than bare $CoSb_2$ due to the incorporation of graphene. Compared with CoSb (or CoSb/G), $CoSb_2$ (or $CoSb_2$/G) yields a higher Li-storage capacity due to its higher Sb-to-Co atomic ratio. The capacity of $CoSb_2$ (or CoSb) is based on the reaction of Li with Li-active Sb to form Li_3Sb that is dispersed in Li-inert Co matrix ($CoSb_2 + 6Li \rightarrow Co + 2Li_3Sb$, $CoSb + 3Li \rightarrow Co + Li_3Sb$) [38,46]. Fig. 6b compares the CV plots between $CoSb_2$ and $CoSb_2$/G. After the first scan, the almost overlapped plots and the fixed peak potentials also indicate an improved electrochemical reversibility of $CoSb_2$ nanocrystals owing to the dispersing and conducting effects of graphene. The small reduction peak at around 0.7 V in the first scan is related to the formation of the solid electrolyte interface (SEI) layer resulting from the irreversible electrolyte decomposition reaction.

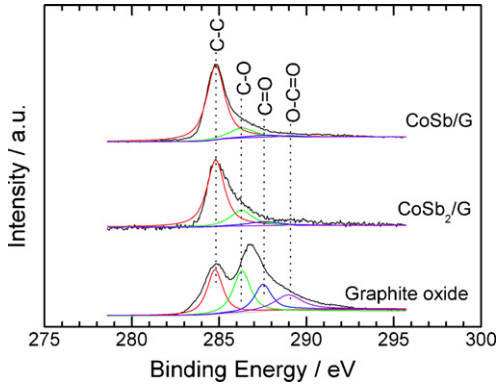

Fig. 4. C 1s XPS of CoSb/G, $CoSb_2$/G and graphite oxide.

The cycling stability of bare $CoSb_2$ and $CoSb_2$/G is compared in Fig. 6c. Clearly, $CoSb_2$/G exhibits an enhanced cycling stability compared to bare $CoSb_2$. After 50 cycles, a charge capacity of 369 mAh g^{-1} is still maintained for $CoSb_2$/G. In contrast, the capacity of bare $CoSb_2$ fades rapidly to 51 mAh g^{-1} after the same cycles. The buffering and confining effects of graphene are considered to be responsible for the better cycling stability of $CoSb_2$/G. It suggests that the graphene itself should have a minor effect on the cycling stability of $CoSb_2$ because the nanocomposite has a low weight ratio of graphene (around 7 wt.% by carbon content analysis) and graphene itself shows an observable capacity fade upon repeated cycling (Fig. 5d). It is noted that $CoSb_2$/G shows a more stable cycling than CoSb/G, which seems not logical since CoSb has a higher Co-to-Sb molar ratio than $CoSb_2$. In this work, the more

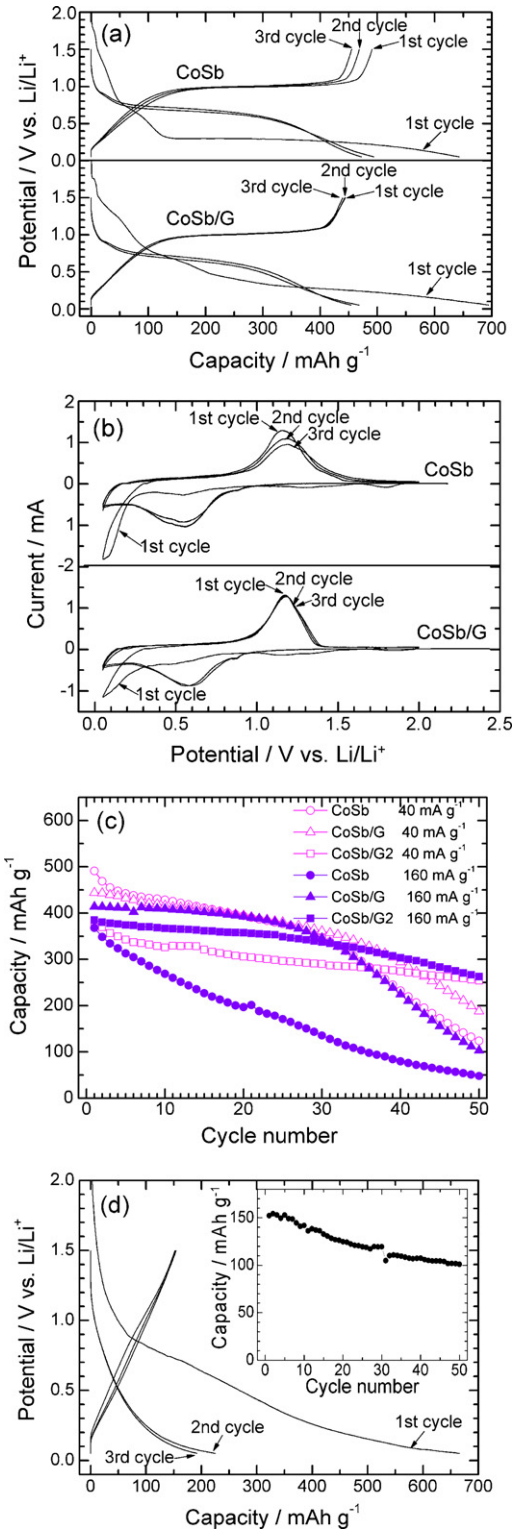

Fig. 5. Electrochemical properties of the solvothermal products: (a) charge–discharge curves at 40 mA g^{-1}, (b) CV plots at 0.1 mV s^{-1} of CoSb and CoSb/G, (c) comparison of cycling stability among CoSb, CoSb/G and CoSb/G2 at 40 and 160 mA g^{-1}, and (d) cycling performance of graphene at 40 mA g^{-1}.

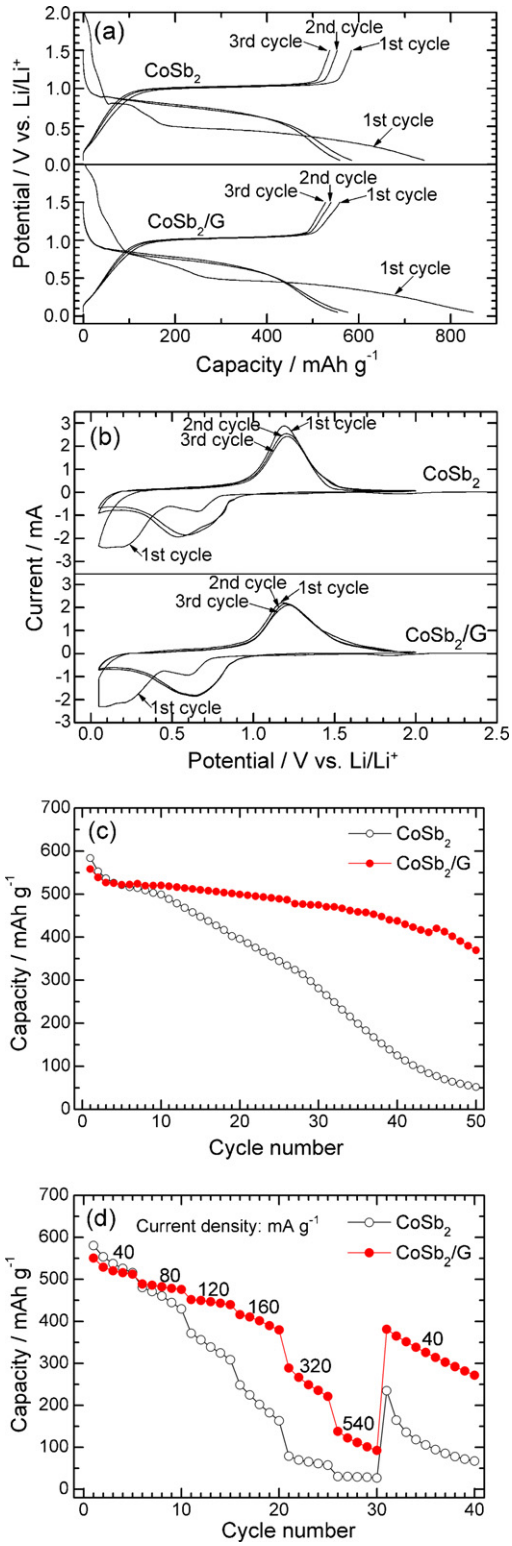

Fig. 6. Electrochemical properties of the solvothermal products: (a) charge–discharge curves at 40 mA g^{-1}, (b) CV plots at 0.1 mV s^{-1} of $CoSb_2$ and $CoSb_2$/G, comparison of (c) cycling stability at 40 mA g^{-1} and (d) rate capability between $CoSb_2$ and $CoSb_2$/G.

stable cycling of $CoSb_2$/G is possibly due to its smaller size and more uniform size distribution compared with CoSb as shown in Figs. 2c and 3c.

Fig. 6d compares the rate capability between $CoSb_2$ and $CoSb_2$/G. It is obvious that the rate capability of $CoSb_2$ can be considerably improved by loading it onto graphene. The enhancement in rate capability comes mainly from two factors: first, the highly conductive graphene offers a 2D conducting channel for the $CoSb_2$ nanoparticles; second, the layered structure of $CoSb_2$/G

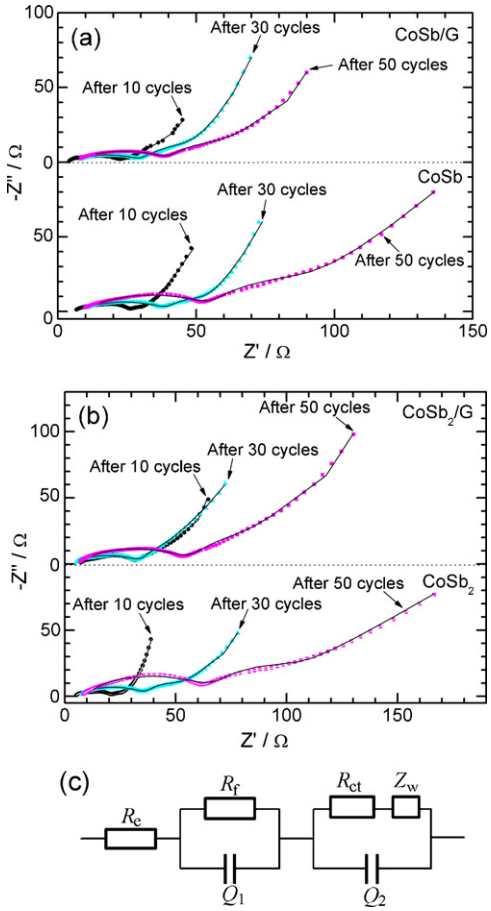

Fig. 7. Nyquist plots of (a) CoSb-based and (b) $CoSb_2$-based electrodes after 10, 30 and 50 cycles, and (c) equivalent circuit.

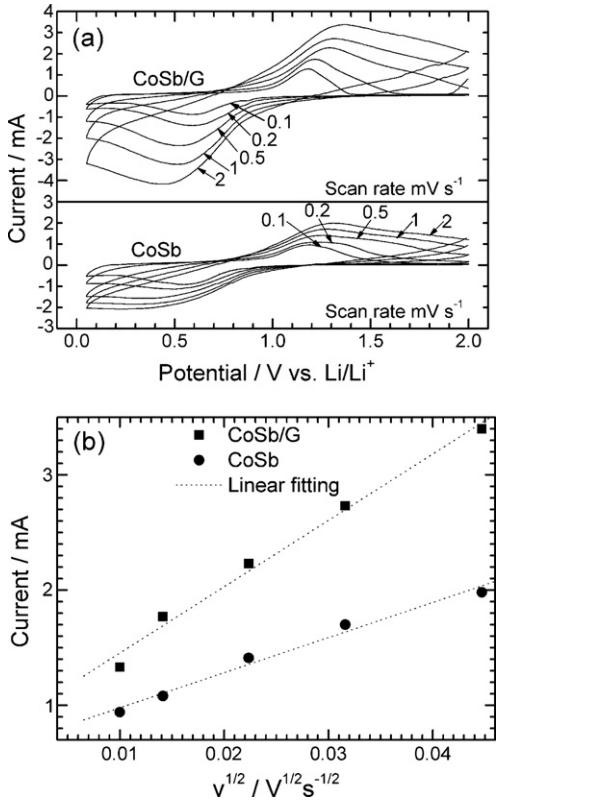

Fig. 8. (a) CV plots of CoSb/G at various scan rates and (b) I_p as a function of $v^{1/2}$ and the corresponding linear fitting.

facilitates the good wetting of the active material by the electrolyte and the rapid Li-ion diffusion at the electrode/electrolyte interface.

EIS was used to obtain a better understanding of the effect of graphene on the electrochemical performance of CoSb and $CoSb_2$. Fig. 7a and b present the Nyquist plots of the CoSb-based and $CoSb_2$-based electrodes after different cycles. The plots consist of a depressed semicircle in the high-to-middle frequency region and a slopping line in the low frequency region. It is generally accepted that the depressed semicircle is actually composed of two partially overlapped semicircles, associated with the Li-ion diffusion across the SEI layer and the charge transfer reaction. The slopping line in the low frequency region is related to the Li-ion solid state diffusion in the bulk electrode. The Nyquist plots are fitted by the equivalent circuit as shown in Fig. 7c. In the equivalent circuit, R_e represents electrolyte resistance, R_f and Q_1 represent SEI layer resistance and the corresponding capacitance, R_{ct} and Q_2 denote the charge transfer resistance and the double layer capacitance, and Z_w is the bulk diffusion resistance. A constant phase element (CPE, denoted by Q_1 and Q_2) instead of a capacitor (C) is used due to the dispersion effect. The CPE can be expressed as [47]:

$$Y_{CPE} = Y_c\omega^n \cos\left(\frac{n\pi}{n}\right) + jY_c\omega^n \sin\left(\frac{n\pi}{n}\right) \quad (1)$$

where ω (=$2\pi f$, f is the frequency) is the angular frequency and $j=(-1)^{1/2}$.

The fitting results are summarized in Table 1. Note that both CoSb/G and $CoSb_2$/G demonstrate a small change in R_f especially in the initial 30 cycles, indicative of a stable microstructure of the SEI layer. By contrast, the relatively large change in R_f for bare CoSb and $CoSb_2$ electrode implies that the microstructure of the SEI layer is subjected to a significant change upon cycling. The change is likely caused by the decomposition of the pristine SEI layer and the formation of new one. This result suggests that the graphene plays an important role in stabilizing the SEI layer. During the initial 30 cycles, CoSb/G and $CoSb_2$/G also exhibit a smaller change in R_{ct} than bare CoSb and bare $CoSb_2$. This means that a stable electrode/electrolyte interface has been established due to the effective confinement of the nanoparticles by graphene. For bare CoSb or bare $CoSb_2$, however, the aggregation of the nanoparticles results in retarded Li-ion diffusion and sluggish electrochemical kinetics. It should be noted that CoSb/G and $CoSb_2$/G also exhibit an increase in both R_f and R_{ct} after cycled for 50 times. This result agrees with the fact that CoSb/G and $CoSb_2$/G also show gradually degraded cycling stability during cycling even though in the presence of graphene. Thus, the microstructure of the hybrids should be optimized to further improve the electrochemical properties.

Li-ion chemical diffusion coefficients, $\tilde{D}_{Li}$, were measured to further understand the mechanism for the improved electrochemical performance by graphene incorporation. The chemical diffusion coefficients were determined using the CV method. Fig. 8a shows the CV plots of the CoSb and CoSb/G electrodes at various scan rates. The symmetry of the plots for bare CoSb degrades progressively with increasing the scan rate. For CoSb/G, on the contrary, the symmetry of the redox peaks is well maintained with the scan rate, indicating the enhanced electrode kinetics by introducing the conductive graphene. Fig. 8b gives the peak current (I_p) as a function of square root of the scan rate ($v^{1/2}$). Note that I_p exhibits a linear relationship with $v^{1/2}$, which is expected for a diffusion-controlled process. The chemical diffusion coefficients can be calculated using the following equation [48]:

$$I_p = 2.69 \times 10^5\, n^{3/2}\, \tilde{D}_{Li}^{1/2}\, C\, v^{1/2} \quad (2)$$

Table 1
Fitting results of the Nyquist plots using the equivalent circuit.

Sample	R_e (Ω)	R_f (Ω)	Q_1		R_{ct} (Ω)	Q_2	
			Y	n		Y	n
CoSb/G							
10 cycles	2.3	4.2	0.105	0.87	22.9	9.1×10^{-4}	0.45
30 cycles	4.5	14.1	1.4×10^{-2}	0.93	27.5	6.6×10^{-4}	0.42
50 cycles	5.2	22.2	9.3×10^{-3}	0.88	37.0	3.7×10^{-4}	0.48
CoSb							
10 cycles	5.9	7.4	3.5×10^{-2}	0.89	22.2	5.1×10^{-4}	0.52
30 cycles	6.8	18.0	2.1×10^{-2}	0.84	34.4	5.1×10^{-4}	0.45
50 cycles	9.6	31.7	5.3×10^{-3}	0.94	48.4	2.5×10^{-4}	0.54
$CoSb_2$/G							
10 cycles	5.9	5.3	3.8×10^{-2}	0.92	29.5	6.8×10^{-4}	0.48
30 cycles	3.9	4.6	5.5×10^{-2}	0.91	31.5	5.1×10^{-4}	0.49
50 cycles	3.8	15.3	2.2×10^{-2}	0.88	54.7	2.6×10^{-4}	0.51
$CoSb_2$							
10 cycles	3.4	5.1	5.8×10^{-2}	0.76	19.6	8.2×10^{-4}	0.46
30 cycles	5.0	11.2	1.4×10^{-2}	0.92	33.1	3.6×10^{-4}	0.50
50 cycles	7.8	21.3	6.9×10^{-2}	0.97	59.5	1.6×10^{-2}	0.59

where n and C represent the charge transfer number and the concentration of the reactant, respectively. The $\tilde{D}_{Li}$ values of CoSb and CoSb/G are 3.7×10^{-12} and 1.3×10^{-11} $cm^2\ s^{-1}$, respectively. $CoSb_2$/G also exhibits a higher $\tilde{D}_{Li}$ value than bare $CoSb_2$ determined using the same method. It is suggested that the unique layered structure is responsible to the increased Li-ion diffusion rate. As a result, the results of EIS and diffusion coefficients can explain the different electrochemical behaviors of the alloy electrodes with and without graphene.

4. Conclusions

In summary, CoSb/G and $CoSb_2$/G nanocomposites have been successfully synthesized by a facile one-pot solvothermal route. CoSb or $CoSb_2$ nanoparticles are uniformly anchored on graphene, forming a unique hybrid nanostructure. Both CoSb/G and $CoSb_2$/G show improved electrochemical properties compared to the bare CoSb and bare $CoSb_2$. The improvement in electrochemical properties is attributed to the incorporation of the flexible graphene that acts both as a buffer to alleviate the volume changes and as a separator to hinder the aggregation of alloy nanoparticles. In addition, the introduced graphene also offers a 2D conductive network and uniformly disperses the nanoparticles, leading to enhanced electrochemical reaction kinetics. The results clearly indicate that graphene plays a crucial role in improving the electrochemical performance of the Co—Sb nanocrystals with potential application as anodes for Li-ion batteries.

Acknowledgements

This work was supported by Zijin Program of Zhejiang University, the Fundamental Research Funds for the Central Universities (No. 2010QNA4003), the Ph.D. Programs Foundation of Ministry of Education of China (No. 20100101120024), the Foundation of Education Office of Zhejiang Province (No. Y201016484), the Qianjiang Talents Project of Science Technology Department of Zhejiang Province (2011R10021), and the National Natural Science Foundation of China (No. 51101139).

References

[1] K.S. Novoselov, A.K. Geim, S.V. Morozov, D. Jiang, Y. Zhang, S.V. Dubonos, I.V. Grigorieva, A.A. Firsov, Science 306 (2004) 666–669.
[2] K.S. Novoselov, A.K. Geim, S.V. Morozov, D. Jiang, M.I. Katsnelson, I.V. Grigorieva, S.V. Dubonos, A.A. Firsov, Nature 438 (2005) 197–200.
[3] A.K. Geim, K.S. Novoselov, Nat. Mater. 6 (2007) 183–191.
[4] S. Park, J.H. An, I.W. Jung, R.D. Piner, S.J. An, X.S. Li, Nano Lett. 9 (2009) 1593–1597.
[5] M.D. Stoller, S. Park, Y.W. Zhu, J.H. An, R.S. Ruoff, Nano Lett. 8 (2008) 3498–3502.
[6] C. Lee, X.D. Wei, J.W. Kysar, J. Hone, Science 321 (2008) 385–388.
[7] I.V. Lightcap, T.H. Kosel, P.V. Kamat, Nano Lett. 10 (2010) 577–583.
[8] Y.F. Li, Z. Zhou, G.T. Yu, W. Chen, Z.F. Chen, J. Phys. Chem. C 114 (2010) 6250–6254.
[9] J.W. Zhu, G.Y. Zeng, F.D. Nie, X.M. Xu, S. Chen, Q.F. Han, X. Wang, Nanoscale 2 (2010) 988–994.
[10] W.J. Hong, H. Bai, Y.X. Xu, Z.Y. Yao, Z.Z. Gu, G.Q. Shi, J. Phys. Chem. C 114 (2010) 1822–1926.
[11] Y.C. Si, E.T. Samulski, Chem. Mater. 20 (2008) 6792–6797.
[12] B. Seger, P.V. Kamat, J. Phys. Chem. C: Lett. 113 (2009) 7990–7995.
[13] N.G. Shang, P. Papakonstantinou, P. Wang, S.R.P. Silva, J. Phys. Chem. C 114 (2010) 15837–15841.
[14] A. Vadivel Murugan, T. Muraliganth, A. Manthiram, Chem. Mater. 21 (2009) 5004–5006.
[15] Z.S. Wu, W.C. Ren, D.W. Wang, F. Li, B.L. Liu, H.M. Cheng, ACS Nano 4 (2010) 5835–5842.
[16] S. Stankovich, D.A. Dikin, G.H.B. Dommett, K.M. Kohlhaas, E.J. Zimney, E.A. Stach, R.D. Piner, S.T. Nguyen, R.S. Ruoff, Nature 442 (2006) 282–286.
[17] G.X. Wang, B. Wang, X.L. Wang, J. Park, S.X. Dou, H. Ahn, K. Kim, J. Mater. Chem. 19 (2009) 8378–8384.
[18] S.Z. Liang, X.F. Zhu, P.C. Lian, W.S. Yang, H.H. Wang, J. Solid State Chem. 184 (2011) 1400–1404.
[19] J.K. Lee, K.B. Smith, C.M. Hayner, H.H. Kung, Chem. Commun. 46 (2010) 2025–2027.
[20] S.L. Chou, J.Z. Wang, M. Choucair, H.K. Liu, J.A. Stride, S.X. Dou, Electrochem. Commun. 12 (2010) 303–306.
[21] J. Yao, X.P. Shen, B. Wang, H.K. Liu, G.X. Wang, Electrochem. Commun. 11 (2009) 1849–1952.
[22] S.M. Paek, E. Yoo, I. Honma, Nano Lett. 9 (2009) 72–75.
[23] L.S. Zhang, L.Y. Jiang, H.J. Yan, W.D. Wang, W. Wang, W.G. Song, Y.G. Guo, L.J. Wan, J. Mater. Chem. 20 (2010) 5462–5467.
[24] Y.M. Li, X.J. Lv, J. Lu, J.H. Li, J. Phys. Chem. C 114 (2010) 21770–21774.
[25] D.H. Wang, R. Kou, D.W. Choi, Z.G. Yang, Z.M. Nie, J. Li, L.V. Saraf, D.H. Hu, J.G. Zhang, G.L. Graff, J. Liu, M.A. Pope, I.A. Aksay, ACS Nano 4 (2010) 1587–1595.
[26] X.Y. Wang, X.F. Zhou, K. Yao, J.G. Zhang, Z.P. Liu, Carbon 49 (2011) 133–139.
[27] S.Q. Chen, P. Chen, M.H. Wu, D.Y. Pan, Y. Wang, Electrochem. Commun. 12 (2010) 1302–1306.
[28] K.H. Seng, Z.P. Guo, Z.X. Chen, H.K. Liu, Adv. Sci. Lett. 4 (2011) 18–23.
[29] E. Yoo, J. Kim, E. Hosono, H.S. Zhou, T. Kudo, I. Honma, Nano Lett. 8 (2008) 2277–2282.
[30] J.I. Paredes, S. Villar-Rodil, A. Martínez-Alonso, J.M.D. Tascón, Langmuir 24 (2008) 10560–10564.
[31] D. Li, M.B. Müller, S. Gilje, R.B. Kaner, G.G. Wallace, Nat. Nanotechnol. 3 (2008) 101–105.
[32] S. Park, R.S. Ruoff, Nat. Nanotechnol. 4 (2009) 217–224.
[33] C. Nethravathi, M. Rajamathi, Carbon 46 (2008) 1994–1998.
[34] H.L. Wang, J.T. Robinson, X.L. Li, H.J. Dai, J. Am. Chem. Soc. 131 (2009) 9910–9911.
[35] Y.X. Xu, K.X. Sheng, C. Li, G.Q. Shi, ACS Nano 4 (2010) 4324–4330.
[36] Z.Y. Lin, Y.G. Yao, Z. Li, Y. Liu, Z. Li, C.P. Wong, J. Phys. Chem. C 114 (2010) 14819–14825.
[37] J. Xie, X.B. Zhao, G.S. Cao, M.J. Zhao, S.F. Su, J. Power Sources 140 (2005) 350–354.
[38] J. Xie, X.B. Zhao, G.S. Cao, Y.D. Zhong, M.J. Zhao, J.P. Tu, Electrochim. Acta 50 (2005) 1903–1907.
[39] L. Kumari, W.Z. Li, J.Y. Huang, P.P. Provencio, J. Phys. Chem. C 114 (2010) 9573–9579.

[40] R.E. Cable, R.E. Schaak, Chem. Mater. 17 (2005) 6835–6841.
[41] W.S. Hummers, R.E. Offeman, J. Am. Chem. Soc. 80 (1958) 1339.
[42] S. Stankovich, R.D. Piner, X.Q. Chen, N.Q. Wu, S.T. Nguyen, R.S. Ruoff, J. Mater. Chem. 16 (2006) 155–158.
[43] S. Stankovich, D.A. Dikin, R.D. Piner, K.A. Kohlhaas, A. Kleinhammes, Y.Y. Jia, Y. Wu, S.T. Nguyen, R.S. Ruoff, Carbon 45 (2007) 1558–1565.
[44] X.F. Guo, J. Jang, S. Nagase, J. Phys. Chem. C 114 (2010) 832–842.
[45] H.J. Shin, K.K. Kim, A. Benayad, S.M. Yoon, H.K. Park, I.S. Jung, M.H. Jin, H.K. Jeong, J.M. Kim, J.Y. Choi, Y.H. Lee, Adv. Funct. Mater. 19 (2009) 1987–1992.
[46] J. Xie, G.S. Cao, X.B. Zhao, M.J. Zhao, Y.D. Zhong, L.Z. Deng, Y.H. Guan, Z.T. Wu, J. Mater. Sci. 39 (2004) 1105.
[47] T. Piao, S.M. Park, C.H. Doh, S.J. Moon, J. Electrochem. Soc. 146 (1999) 2794–2798.
[48] Y. Shi, L. Wen, F. Li, H.M. Cheng, J. Power Sources 196 (2011) 8610–8617.